Multi-angle Observations of Arctic Clouds from FIRE ACE:

June 3, 1998 Case Study

Roger T. Marchand and Thomas P. Ackerman

Pacific Northwest National Laboratory, Richland, WA 99352

Michael D King

NASA Goddard Space Flight Center, Greenbelt, MD 20771

Catherine Moroney

Institute of Atmospheric Physics, University of Arizona, Tucson, AZ 85721-0081

Peter Muller

Department of Geomatic engineering, University College London, London, United Kingdom

Abstract. In May and June of 1998, the Airborne Multi-angle Imaging Spectro-Radiometer (AirMISR) participated in the FIRE Arctic Cloud Experiment (ACE). AirMISR is an airborne instrument for obtaining multi-angle imagery similar to that of the satellite-borne MISR instrument. This paper presents a detailed analysis of the data collected on June 3, 1998. In particular, AirMISR radiance measurements are compared with measurements made by two other instruments, the Cloud Absorption Radiometer (CAR) and the MODIS airborne simulator (MAS), as well as to plane-parallel radiative transfer simulations. It is found that the AirMISR radiance measurements and albedo estimates compare favorably both with the other instruments and with the radiative transfer simulations. In addition to radiance and albedo, the multi-angle AirMISR data can be used to obtain estimates of cloud top height using stereo-imaging techniques. Comparison of AirMISR retrieved cloud top height shows excellent agreement with the measurements from the airborne Cloud Lidar System (CLS) and ground-based millimeter-wave cloud radar.

1. Introduction

In May and June of 1998, the Airborne Multi-angle Imaging Spectro-Radiometer (AirMISR) participated in the FIRE Arctic Cloud Experiment (ACE). AirMISR is an airborne instrument for obtaining multi-angle imagery similar to that of the satellite-borne MISR instrument [Diner et al. 1998]. MISR is one of five instruments on board the NASA Terra platform (previously known as EOS-AM1). During the FIRE ACE experiment, 13 flights (each with 4 to 8 AirMISR data acquisitions or runs) were attempted over Point Barrow, Alaska or the Surface HEat Balance of the Arctic Ocean (SHEBA) ice station. In the SHEBA experiment, the Canadian Coast Guard icebreaker Des Groseilliers was frozen in the pack ice of the Arctic Ocean. Starting roughly 300 miles north of Alaska and 900 miles south of the North Pole, the Des Groseilliers spent one year drifting with the pack ice [Curry et al., 1999].

AirMISR flies on the NASA ER-2 aircraft and has a single pushbroom (line imaging) camera of the same design as the nine cameras on the MISR satellite-based instrument. High resolution images are obtained by this camera in four narrow spectral bands centered at 446, 558, 672, and 866 nm [Bruegge et al., 1998]. The AirMISR camera can be adjusted in flight to point from $+70.5^{o}$ to -70.5^{o} relative to nadir along the direction of flight. By rotating at specific times, the camera obtains images of the same target from a variety of angles. During the FIRE ACE experiment, the camera was adjusted to reproduce the nine view angles which will be obtained by the satellite (that is a nadir view plus 26.1, 45.6, 60.0, and 70.5 degrees forward and aft). Image resolution is approximately 7 meters at nadir (with a cross track image width of approximately 10 km) and 21 meters at 70.5^{o}. Figure 1, for example, shows the 866 nm nadir and forward +26.1 degree views obtain during one pass over the SHEBA ground site (i.e. the Canadian Coast Guard icebreaker Des Groseilliers) on 3 June 1998.

This paper presents a detailed analysis of AirMISR data collected on June 3, 1998. In particular the paper examines AirMISR radiance measurements, as well as retrievals of cloud albedo and cloud top height. This case study is the first step in a program to validate MISR cloud retrievals. The results are encouraging as the AirMISR measurements and retrievals are found to compare very favorably with those of other instruments and with simulations based on a combination of in situ and ground-based measurements.

After a brief description of the June 3 case in section II, section III compares AirMISR radiances measurements with radiance measurements from the Cloud Absorption Radiometer (CAR) [King et al., 1986], on board the University of Washington CV-580, the Moderate resolution imaging spectroradiometer Airborne Simulator (MAS) [King et al., 1996] and with radiative transfer simulations. Both the CAR and MAS instruments make measurement near 672 and 866 nm and this study focuses on these wavelengths.

The nine MISR satellite radiance measurements will routinely be used to estimate cloud albedo at the four MISR wavelengths. Section IV compares the MISR albedo retrievals with measurements from the CAR instrument, as well as the Solar Spectral Flux Radiometer (SSFR), which was also on board the University of Washington CV-580. Finally, stereo-imaging techniques can also be applied to image pairs, such as those shown in figure 1, in order to determine the height of observed features such as cloud tops. The MISR program plans to use stereo-based height retrievals to both help determine when clouds are present, as well as to determine the cloud top height. (It is also important to know the position of reflecting surfaces, so that measurements of the upwelling radiances at all angles can be geometrically co-registered to the correct common point). Section V compares AirMISR retrieved cloud top height with that

measured from the airborne Cloud Lidar System (CLS), which was on board the NASA ER-2, and from ground-based millimeter-wave cloud radar.

2. Description of the June 3 Case

From 31 May until 11 June, the SHEBA station was between a surface low to the northwest and the Beaufort high, which was far to the east. The ship was typically under southerly winds which brought some fog and drizzle on 5 and 7 June, while some light snow occurred on 9 and 11 June (personal communication Don Wylie, University of Wisconsin-Madison). On 3 June, the SHEBA site was under southeasterly winds and was overcast by stratus clouds for more than 24 hours proceeding the overpasses of the ER-2. For much of this time the cloud was multilayered with the top of the highest layer near 3 km.

Figure 2 shows reflectivity data from the vertically pointing millimeter-wave cloud radar on board the Des Groseilliers for the several hours surrounding the ER-2 overpasses (data provided by Taneil Uttal, Environment Technology Laboratory). Multi-layer stratus clouds persisted over the ship until about 22 UTC (universal time) after which time there is no lower cloud. The millimeter-wave radar reflectivity is proportional to the sixth moment of the droplet size and therefore very sensitive to drizzle. Much of the reflectivity associated with the upper cloud (that is, the relatively high reflectivity region extending from 3 km to just below 2 km) is drizzle. Cloud base of the upper cloud was between 2.5 and 2.8 km as revealed by ground-based lidar, radar Doppler velocity, and in situ measurements.

In simulations presented in the next section, cloud base of the upper cloud was taken as 2.7 km when lidar estimates were not available as a result of attenuation due to the lower cloud.

Although cirrus clouds were observed earlier in the day, neither the ground-based millimeter-wave radar nor the Cloud Lidar System (CLS) on the ER-2 detected any cirrus in the vicinity of the ship at the time of the ER-2 overpasses.

The University of Washington CV-580 conducted in situ measurements during one descent, at approximately 21:20 UTC, and one ascent at approximately 22:15 UTC near the SHEBA ship. Figures 3 and 4 show the mean effective radius and liquid water content measured by a Particle Measuring Systems Model FSSP-100 and a Gerber Scientific Instruments PVM-100A (data provided by Peter Hobbs, University of Washington, and Hermann Gerber, Gerber Scientific Inc.) [Gerber et al., 1994]. During the descent, the CV-580 passed through two cloud layers with most of the liquid water contained in the upper cloud layer. In the upper cloud layer, both instruments show an effective radius which increased from about 6 microns at cloud base to about 10 microns at cloud top. Both instruments also showed a standard deviation in the effective radius of roughly one micron during the descent and a somewhat larger standard deviation during the ascent. In the lower cloud, which was sampled only during the descent, both probes showed an effective radius between about 5 and 8 microns with a standard deviation of about two microns.

During both the descent and ascent, the FSSP detected a few relatively large particles just below cloud base (consistent with the radar observation). Some of these particles may have been ice. Be that as it may, the depolarization lidar on the SHEBA ship revealed depolarization ratios for both clouds which are typical of water drops. It seems likely that the clouds were predominately composed of liquid water.

3. **Upwelling Radiance and Broadband Surface Flux**

Figure 5 shows the upwelling radiance measured by the Cloud Absorption Radiometer (CAR) (data provided by Michael King and Jason Li, Goddard Space Flight Center). In figure 5, the radiance is expressed as a bi-directional reflectance factor (BRF), which is simply the ratio of the measured radiance to what would be measured from a perfectly reflecting lambertian surface.

CAR is a multi-wavelength scanning radiometer that measures the angular distribution of scattered radiation [King et al., 1986, King, 1992 and Tsay et al., 1998]. During the FIRE ACE experiment, the CAR instrument was housed in the nose of the University of Washington CV-580. The instrument has a mirror that scans in a plane perpendicular to the direction of flight through a 190° opening. By flying in a circular pattern (the flight path is depicted in figure 6) and scanning from just before zenith to just past nadir a composite of the upwelling and downwelling radiance fields can be constructed. In figure 5, the composite was created by binning the measurements into 1^o x 1^o cells and taking the median value in each cell. The data have been corrected for pitch[1] and roll of the CV-580 as outlined by King [1987]. Because of the aircraft pitch, however, there is a small region near nadir (the center of the pattern) that was not observed by the radiometer.

Figure 7 shows that a similar BRF can be obtained using plane parallel radiative transfer calculations. These calculations were done using the Spherical Harmonics Discrete Ordinate Method (SHDOM) [Frank Evans, 1998]. The calculation shown used cloud boundaries estimated from radar and lidar data, as described in the previous section. The liquid water

[1] The instrument on board the CV-580 that measures the aircraft pitch (i.e., the Trimble TANS/Vector GPS Altitude System) did not function properly during this portion of the flight. After discussions with Peter Hobbs, a best guess pitch of 5^o was used. After inclusion of a correction factor to account for the alignment of the CAR instrument relative to the aircraft (as measured by Jason Li, Goddard Space Flight Center), we have great confidence that resulting CAR pointing is good to approximately 1 degree, since the pointing correction results in the sun being located precisely where ephemeris calculations indicate it should.

content was set to linearly increase in height (from zero at cloud base) with the total liquid water path set to the value obtained from a passive microwave radiometer at the SHEBA site[2]. Three quarters of the liquid water was placed in the upper cloud. In the upper cloud, the cloud droplet effective radius was set to increase linearly from 6 microns at cloud base to 10 microns at cloud top. One quarter of the liquid water was placed in the lower cloud with a constant effective radius of 7 microns. These distributions are consistent with the in situ measurements discussed in the previous section.

The radiative transfer calculations are significantly influenced by the highly reflective sea ice. Although there was not a great deal of snow on the ice surface by this time, there were few (if any) melt ponds and little open water or new ice (less than 2%)[3]. Figure 8 depicts the average spectral surface albedo measured by Don Perovich on June 3 and the model spectral albedo used in the radiative transfer calculations [Perovich, 1994]. This model yields a broadband albedo of 0.71 (under cloudy conditions).

Turning attention to the surface flux, figure 9 shows the downward shortwave broadband flux measured at the SHEBA ship and at three of the NCAR portable automated mesonet (PAM-III) stations. The position of the PAM stations and the SHEBA ship are given in figure 6. Figure 9 shows that the simulation agrees well with the measurements from 20 UTC until after 21 UTC. After 21 UTC, the measured flux begins to greatly exceed the simulated value. All four radiometers show this increase in downward flux, but the southern most station (Baltimore)

[2] A two channel microwave radiometer was supplied by the Department of Energy Atmospheric Radiation Measurement (ARM) program for this experiment. During this portion of the experiment, the radiometer was operating in a tip (or scanning) mode which requires a couple of minutes to obtain a complete set of data from which to retrieve cloud liquid water path and water vapor path. The liquid water retrieval used in this study assumes the liquid water temperature to be equal to the air temperature (between 2.8 and 3 km) as measured by a radiosonde (i.e. balloon). This approach differs from the standard ARM approach which is based on a statistical technique. Since the water was higher and hence colder than the "typical" case, the liquid water path used here is 20 to 25% lower than what is obtain using the statistical approach.

shows the effect earlier than the other sites[4]. Data from the MODIS Airborne Simulator (MAS) show what appears to be a region of very thin clouds south (that is downwind) of the ship and although it is not very obvious in figure 6 the southern portion of the AirMISR cloud scene is in fact brighter than the northern half. It seems likely that the cloudy region in the southern portion of figure 1 is optically thinner than the region to the north. It is also possible that because the sea ice is highly reflective (allowing for significant multiple scattering of photons between the surface and the clouds) and because the thin cloud region is in the direction of the sun (sea ice usually has a strong scattering component near the specular direction), that there may be a significant increase in the surface flux due to horizontal transport of photons after 21 UTC.

Taking a closer look at the measured and simulated radiances, figure 10 compares the radiative transfer simulation to the CAR, AirMISR, and MAS radiance measurements in the azimuthal plane observed by AirMISR (i.e., along the direction of flight of the ER-2). That is, figure 10 represents a cut plane or slice removed from figures 5 and 7. The figure shows that the AirMISR measurements agree extremely well with those of the CAR instrument (solid line) and the MAS data[5].

It should be stressed that the CAR measurements began approximately two minutes after the first overpass by the ER-2, and even if the timing had been more precise CAR would not be sampling exactly the same cloud region. As a rough measure of the variability one might expect due to observing differing areas of the cloud scene, the light dotted line in figure 10 shows one

---

[3] Personal communication Don Perovich, Cold Regions Research and Engineering Laboratory, and Judy Curry, University of Colorado.

[4] The ARM measurement (located at the ship) is consistently higher than the nearby Seattle and Atlanta PAM stations before the overflilght of the ER-2. The reasons for this are unclear. We note, however, a reduction in the cloud liquid water path by 20% or an increase in effective radius by 20% (or a combination of the two) increases the simulated flux sufficiently to agree closely with the ARM radiometer. A combined error of 20% in the estimate for these quantities is very plausible and so the closer agreement of the simulation with the PAM data does not necessarily suggest that the ARM radiometer is incorrect.

standard deviation in the composite CAR BRF. The error bars on the AirMISR measurements, on the other hand, represent the 3% absolute calibration uncertainty for this instrument, which is larger than the standard deviation in the measured radiances.

In addition to sampling issues, CAR was flying on the CV-580 only a few hundred meters above cloud top, whereas AirMISR and MAS were about 17 km above the clouds. However, in the absence of absorbing aerosols above the cloud layer, the only significant change in the upwelling radiance at this wavelength is due to Rayleigh scattering and absorption by ozone[6]. The simulations show that except near the forward scattering direction, the difference between 3.5 km and 20 km is not significant. Measurements and simulations near 870 nm (figure 11) show much the same pattern as those near 670 nm (figure 10), except of course, ozone and Rayleigh scattering have no appreciable effect.

The simulations shown in figure 10 and 11 include a small amount of aerosol (optical depth of about 0.1 at 500 nm). This optical depth is consistent with measurements obtained from a Multi-Filter Rotating Shadow Band Radiometer (MFRSR) on the nearest clear sky days of May 23 and 24. In the model, the aerosol was uniformly distributed between the surface and two kilometers, and the aerosol properties were chosen to be consistent with D'Almedia et al. [1991 (see tables 43b and 44b)] for summer Arctic aerosol (Asymmetry parameter 0.689 and single scattering albedo 0.884 at 672 nm). The aerosol has only a small effect on the simulations. Without the aerosol, the upwelling radiances increase by about 1 %. The same holds true for the albedo (see also table 1 in the following section).

---

[5] As with the CAR data, the AirMISR and MAS data were binned into 1^o x 1^o cells. The AirMISR and MAS data were also visual aligned to ensure that both data corresponded to the same cloud region.

4. Albedo

One of the goals of the MISR satellite is to use its nine radiance measurements to estimate cloud albedo with greater accuracy than current satellite-based estimates, which effectively use only one such measurement. MISR plans to use three approaches in estimating the cloud albedo.

When a cloud scene is believed to be homogenous, a relationship based on a library of plane-parallel simulations is used to estimate the albedo. The determination of whether or not to use a homogeneous model is based on a combination of the observed heterogeneity of the cloud scene at the several pixel level and on how well the measured radiances fit the pattern of the homogeneous model. When a given pixel does not meet the homogeneous cloud criteria, a heterogeneous cloud model is used which has been created using Monte Carlo simulations of a variety of heterogeneous cloud fields. The applicability of this heterogeneous (or statistical) model is also examined by evaluating how well the pattern of the measured radiances matches the heterogeneous model. The heterogeneous cloud thresholds are less stringent than the homogeneous thresholds. In the event that even the heterogeneous model appears inappropriate, the cloud albedo is estimated assuming that there is no azimuthal variation in the cloud reflection [Tamas et al., 1999, and Diner et al., 1997].

Table 1 summarizes the narrowband albedos as inferred from AirMISR, CAR, and the radiative transfer simulations, as well as that measured by the Solar Spectral Flux Radiometer (SSFR) [Pilewskie et al., 1998] (data provided by, P. Pilewskie, NASA Ames)[7]. It must be

[6] In the simulations, the ozone concentration was set to .397 atm-cm. This is the average value which we inferred using the Langely technique with MFRSR measurements on May 23 and 24 (the nearest time with sufficient clear skies to apply the Langley approach).

[7] In obtaining the SSFR spectral albedo, the CV-580 navigation data was used to isolate periods where the aircraft was near level flight (within ± 2.5 degrees) in both pitch and roll. A moving average filter with an approximately 60 second window was applied to the navigation data to remove occasional spurious readings. At each selected time, the SSFR upwelling and downwelling spectral irradiance were averaged over a period of roughly five minutes before being used to calculate the albedo. (Averaging intervals of 5 to 15 minutes yield very similar results while periods much smaller than 5 minutes yielded similar means but higher standard deviations).

stressed that all of the measurements correspond to somewhat different times and different regions of the cloud field. The CAR results are closest in time to the first AirMISR measurements at 21:02 UTC, and these results are highlighted in the table.

The albedos in Table 1 reported by AirMISR (and by CAR) are defined as the ratio of the measured upwelling irradiance to the downwelling irradiance at the top of atmosphere. Borrowing from MISR nomenclature, these albedos are labeled as "local" albedos. As a result of absorption by ozone and Rayliegh scattering, this albedo should be somewhat lower than the ratio of the upwelling to downwelling at cloud top. The simulations show that this difference is about 3% at 670 nm and negligible at 860 nm.

5. Stereo-Imaging (Cloud Top Height)

In addition to radiance measurements and corresponding albedo estimates, stereo-imaging techniques can be applied to the AirMISR multi-angle data to determine the altitude of observed objects, such as cloud tops [Moroney et al., 1999, Diner et al., 1998]. Figure 12 shows a simple sketch of the basic concept.

A careful inspection of Figure 1 suggests that a number of cloud features appear to have moved between the acquisition of these two AirMISR images. Using an estimate of the actual cloud velocity (obtained from rawinsonde data in this case, but will be obtained by MISR using a third image), this apparent shift in position can be used to extract the cloud top height. Figure 13 shows the stereo-retrieved cloud top height for the image pair in figure 1. For the most part, the cloud top heights displayed in Figure 13 vary between about 2.8 and 3.2 km. Given the uncertainties in the cloud velocity, location and orientation of the ER-2, as well as pointing angle

uncertainties with the AirMISR instrument itself, we estimate that this retrieval should be accurate to approximately 500 meters.

The average cloud top height is consistent with millimeter-wave radar data from the SHEBA ice station (see figure 2), which shows cloud tops very near 3 km for the several hours surrounding the ER-2 overpasses. Further, a careful examination of the stereo-derived cloud top height field shows that the position of the retrieved valleys and peaks are consistent with a visible interpretation of the cloud cell structure.

The retrieval is also consistent with measurements made from the downward looking Cloud Lidar System (CLS), which was being flown on board the ER-2 [Spinhirne et al., 1982]. Figure 14 compares the AirMISR stereo-derived cloud top heights along the ER-2 ground track, with those measured by the lidar. In this figure, the height retrieval using both the full MISR algorithm and only a portion of the algorithm are included.

The first step in the MISR stereo-height retrieval is to identify common features between image pairs. The MISR approach uses a number of image and feature recognition codes (called M2, M3 and Rank Sort) as well as a variable search window. The search window restricts the size of the target image where a matching feature is sought. If one uses a small search window centered on the correct point in the target image, one is unlikely to misalign the features and of course the retrieval works much faster. Figure 14 shows that the lidar and complete MISR algorithm compare very favorably (well with in the estimated 500 meter uncertainty). This cloud scene shows little variability in the cloud top and part of the reason the full algorithm works well in this example is that the search window is reduced in size such that it is unlikely that a poor match will be found. Without the reduced search window the matcher still works well, shown here using only the M2 matcher with a large search window. However, a number of blunders (or

incorrect matches) were encountered. (All those points that do not lie near the lidar cloud top height are blunders caused by incorrect image matching). Many, but not all, of these blunders are detected as blunders by the software. Techniques which will identify the blunders with greater fidelity are currently being investigated by the MISR science team. Several of these techniques make use of consistency between stereo matching of a forward view with nadir and an aftward view with nadir.

Similar results for the cloud top height retrieval were obtained on both AirMISR overpasses and using various possible image pairs from the nadir, ±26.1 and ±45 degree views. Of course, the resolution of the AirMISR images is much higher than the MISR satellite instrument. Be that as it may, the cloud top height retrieval algorithm continued to perform well even after averaging the AirMISR data to match the resolution of MISR, as shown in figures 15 . Figure 15 is the same as figure 14 only that the AirMISR radiance data was averaged to 275 meter resolution prior to attempting the stereo-height retrieval. The finite spatial resolution of the images introduces a quantization of the possible retrieved heights. At the reduced image resolution of 275 meters, the AirMISR quantization (for this example) is more than 500 meters. That is, a one pixel shift in the position of an object (in one image relative to the other) changes its height retrieval by more than 500 meters. In figure 15, the small variations in heights (less than 100 meters) are due to small variations in the aircraft orientation. Those points whose height retrieval is near 3800 meters is a result of only a one pixel error in the imagine matching.

6. Discussion and Summary

This case study is the first step in a program to validate MISR cloud retrievals. A detailed analysis of AirMISR data shows that the radiance measurements, as well as retrievals of cloud

albedo and cloud top height (based on MISR algorithms) are in good agreement with other instruments (CAR, MAS, SSFR, CLS, millimeter cloud radar) and with radiative transfer simulations based on a combination of ground-based and in situ measurements.

With respect to cloud top height, it was observed that the use of a reduced search window improved the algorithm performance. This improvement will only be realized when the cloud top heights are relatively uniform, as in this case. With the reduced search window intentionally removed, the algorithm performed well on average. The only difficulty without the reduced search window was the ability of some poor matches (or blunders) to go undetected. However, it should be stressed that cloud regions with relatively large variations in cloud top height (i.e. those where the reduced search window will not be used) will generally have cloud features which are easier to identify than for this very homogeneous case. In this sense, removing the search window for these data is a strenuous test.

Finally, with respect to cloud albedo it is worth mentioning that despite a highly reflective underlying surface (and considerable multiple scattering of photons between the cloud and the surface), typical arctic aerosols had only a small effect (~1%) on the simulated upwelling radiance and albedo (above cloud top).

Acknowledgements. The authors would like to express their thanks and acknowledge the help of a great many people who made this research possible. Thank you: Tamas Varnai, and Roger Davies at the University of Arizona, as well as, Rowan Dundas at University College London for developing and running the image matching and MISR albedo software. Frank Evans for providing SHDOM and answering lengthy inquires. Jason Li at the Goddard Space Flight Center and Jeff Myers at the NASA Ames Research Center for providing calibrated data from

the Cloud Absorption Radiometer and MODIS Airborne Simulator. Peter Hobbs at University of Washington and Hermann Gerber from Gerber Scientific Inc. for their helpful comments and for providing the in situ cloud data and navigational data for the CV-580. Don Perovich at the Cold Regions Research and Engineering Laboratory for providing the surface spectral albedo data. Taneil Uttal at the Environment Technology Laboratory for providing the millimeter cloud radar data. James Spinhirne and Bill Hart at the Goddard Space Flight Center for providing cloud top heights from the Cloud Lidar System. Judy Curry at the University of Colorado and Don Wylie for at the University of Wisconsin-Madison for their helpful comments. Peter Pilewskie and John Pommier at NASA Ames for providing the Solar Spectral Flux Radiometer data. We thank also our colleagues in the SHEBA Atmospheric Surface Flux group, Ed Andreas, Chris Fairall, Peter Guest, and Ola Persson, for help collecting and processing the PAM data. The National Science Foundation supported this research with grants to the U.S. Army Cold Regions Research and engineering Laboratory, NOAA's Environmental Technology Laboratory, and the Naval Postgraduate School. Last, but not least, thank you to those at the NASA Jet Propulsion Laboratory who made this research possible, Jose D. Garcia, Marco A. Hernandez, William C. Ledeboer, Veljko M. Jovanovic, Bill Cunningham, Carol Bruegge, and others on the MISR project who assisted in the post flight processing.

This research was made possible by support of NASA and the MISR program. We would especially like to thank David Diner for this support, in addition to his helpful comments and insights.

References

Bruegge, Carol J., Valerie G. Duval, Nadine L. Chrien, Robert P. Korechoff, Barbara J. Gaitley, and Eric. B. Hochenberg, 1998 "MISR Prelaunch Instrument Calibration and Characterization Results, *IEEE transactions on Geoscience and Remote Sensing, 36(4),* 1186-1198, 1998.

Curry, J.A., P. Hobbs, M. King, D. Randall, P. Minnis, et al., FIRE Arctic Clouds Experiment. *Bull. Amer. Meteorol. Soc.*, in press (Dec issue), 1999.

D'Almedia, Guillaume A., Peter Koepke, Eric P. Shettle, *ATMOSPHERIC AEROSOLS: Global Climatology and Radiative Characteristics*, A. Deepak Publishing, Hampton, Virginia, USA, 1991.

Diner, David J., Lisa M. Barge, Carol J. Bruegge, Thomas G. Chrien, James E. Conel, Michael L. Eastwood, Jose D. Garcia, Marco A. Hernandez, Charles G. Kurzweil, William C. Ledeboer, Neil D. Pignatano, Charles M. Sarture, and Bruce G. Smith, The Airborne Multi-angle Imaging SpectroRadiometer (AIRMISR): Instrument Description and First Results, *IEEE transactions on Geoscience and Remote Sensing, 36(4)*, 1339-1349,

Diner, D. J., R. Davies, T. Varnai, C. Moroney, C. Borel, ans S.A.W. Gerstl, Multi-angle Imaging SpectroRadiometer level 2 Top-of-Atmosphere Albedo Algorithm Theoretical Basis,

Technical Document JPL D-13401, Jet Propulsion Laboratory, California Institute of Technology, Pasadena, CA, 1997.

Diner, D. J., R. Davies, L. DiGirolamo, A. Horvath, C. Moroney, J.P. Muller, S.R. Paradise, D. Wenkert, and J. Zong, Multi-angle Imaging SpectroRadiometer level 2 Cloud Detection and Classification Algorithm Theoretical Basis, Technical Document JPL D-11399, Jet Propulsion Laboratory, California Institute of Technology, Pasadena, CA, 1998.

Evans, K. F., The spherical harmonics discrete ordinate method for three-dimensional atmospheric radiative transfer, *J. Atmos. Sci., 55,* 429-466, 1998.

Gerber, H., B. G. Arends, and A. S. Ackerman, A new microphysics sensor for aircraft use, *Atmos. Res.*, **32,** 235-252, 1994.

King, M. D., M. G. Strange, P. Leone and L. R. Blaine, Multiwavelength scanning radiometer for airborne measurements of scattered radiation within clouds, *J. Atmos. Oceanic Technol., 3,* 513-522, 1986.

King, Michael D., Determination of the Scaled Optical Thickness of Clouds from Reflected Solar Radiation Measurements, *J. of Atmo. Sci., 44(3),* 1734-51, 1987.

King, M. D., Directional and spectral reflectance of the Kuwait oil-fire smoke. *J. Geophys. Res., 97,* 14545-14549, 1992.

King, M. D., W. P. Menzel, P. S. Grant, J. S. Myers, G. T. Arnold, S. E. Platnick, L. E. Gumley, S. C. Tsay, C. C. Moeller, M. Fitzgerald, K. S. Brown and F. G. Osterwisch, 1996: Airborne scanning spectrometer for remote sensing of cloud, aerosol, water vapor and surface properties. *J. Atmos. Oceanic Technol., 13*, 777-794, 1996.

Moroney, Catherine, Roger Davies, and Roger Marchand, Cloud-Top Heights from AirMISR Stereo Measurements, AMS 10th Conference on Atmospheric Radiation, June 28 - July 2, Madison, WI., p. 110-113, 1999

Pilewskie, Peter, Alexander F.H. Goetz, David A. Beal, Robert W. Bergstrom, and Peter Mariani, Observations of the spectral distribution of solar irradiance at the ground during SUCCESS, *Geophys. Res. Lett., 25(8)*, 1141-1144, 1998.

Perovich, Donald K., Light Reflection from sea ice during the onset of melt, *J. Geophys. Res., 99*, 3351-3359, 1994.

Spinhirne, J. D., M. Z. Hansen, and L. O. Caudill, Cloud top remote sensing by airborne lidar, *Appl. Opt., 22*, 1564-1571, 1982.

Varnai, Tamas, Roger Davies, and Roger Marchand, Evaluating Cloud Albedo Retrieval Algorithms that use Multi-Angle Radiance Measurements, AMS 10th Conference on Atmospheric Radiation, June 28 - July 2, Madison, WI., p. 54-57, 1999

Tsay, S. C., M. D. King, G. T. Arnold, and J. Y. Li, Airborne spectral measurements of surface anisotropy during SCAR-B. *J. Geophys. Res., 103*, 31943-31954, 1998.

List of Figures

Figure 1a – Near-IR (866 nm) nadir view obtained at approximately 21:30 universal time (UTC) on a universal transverse mercator (UTM) projection. The white x denotes the same cloud feature in figures 1a and 1b.

Figure 1b – Near-IR (866 nm) $+26.1^{o}$ (forward looking) view obtained at approximately 21:30 universal time (UTC). The white x denotes the same cloud feature in figures 1a and 1b.

Figure 2 – Radar reflectivity (in dBZ) on 3 June 1998. Multi-layer stratus clouds persisted over the ship until about 22 UTC when the lower cloud dissipated. Much of the reflectivity associated with the upper cloud (that is the relatively high reflectivity region extending from near cloud top to just below 2 km) is drizzle. Cloud base of the upper cloud was between 2.5 and 2.8 km as revealed by ground-based lidar and in situ measurements.

Figure 3 – Effective radius (left panel) and liquid water content (right panel) measured by the FSSP and PVM during decent through the cloud layers at approximately 21:20 UTC.

Figure 4 – Same as figure 3 except during the ascent at approximately 22:15 UTC.

Figure 5 – Upwelling radiance measured by the Cloud Absorption Radiometer. The upwelling is expressed as a bi-directional reflectance factor (BRF), which is simply the ratio of the measured radiance to what would be measured from a perfectly reflecting lambertian surface. The BRF

was determined by binning the radiometer measurements into 1^o x 1^o cells and taking the median value in each direction. The solar zenith angle is approximately 56^o and is located to the right side of the figure. The red band on the left edge of the figure is the forward scattering peak and the large oval feature in the backscattering direction is the "rainbow effect." (Although in this case, the cloud droplets are sufficiently small such that we believe an observer would actually see a "white bow" not a true rainbow).

Figure 6 – AirMISR 672 nm nadir image obtained at approximately 21:02 UTC over the SHEBA ice station (white x) on a universal transverse mercator (UTM) projection. Also shown on this figure are the position of three of the NCAR portable automated mesonet (PAM-III) stations and the flight path of the University of Washington CV-580 during acquisition of the Cloud Absorption Radiometer (CAR) data. (The A or Atlanta PAM station is marked by a white square, the Seattle station by a white circle and the Baltimore station by a white asterisk).

Figure 7 – Simulated upwelling BRF. (As in Figure 5, the solar zenith angle is approximately 56^o and the sun is located to the right side of the figure).

Figure 8 – Modeled and measured surface spectral albedo.

Figure 9 – Simulated and measured broadband shortwave flux at the surface. The measured flux at the SHEBA ICE station and three of the PAM stations is presented. Station B or Baltimore was the southern most station, as depicted in figure 5.

Figure 10 – Modeled and Measured upwelling radiance in the azimuthal plane measured by AirMISR near 670 nm. The light dotted line shows one standard deviation in the CAR measurement, and the error bars show the calibration uncertainty in the AirMISR measurements. The upwelling is expressed as a bi-directional reflectance factor (BRF), which is simply the ratio of the measured radiance to what would be measured from a perfectly reflecting lambertian surface. The solar zenith angle is approximately 56^o and the AirMISR azimuthal plane is 35^o (relative to the sun) for the aftward (negative) viewing angles and 215^o for the forward (positive) viewing angles.

Figure 11 – Modeled and Measured upwelling radiance in the azimuthal plane measured by AirMISR near 860 nm.

Figure 12 – Depiction of the apparent change in position with look angle for an object located above the reference surface.

Figure 13 – Stereo-retrieved cloud top height (in meters) using the full MISR algorithm for the 21:30 UTC overpass of the SHEBA ice station.

Figure 14 – Comparison of stereo-retrieved cloud top height and ER-2 Cloud Lidar System measured cloud top height. Stereo-based results are shown with both the full MISR algorithm (figure 13) and with one that does not include a restricted search window.

Figure 15 – Comparison of stereo-retrieved cloud top heights using images with resolution reduced to 275 meters with the ER-2 Cloud Lidar System measured cloud top height.

	672 nm	866 nm
AirMISR (Local)		
21:02 UTC		
Homogeneous	**0.82 ± ~ 0.03**	**0.78**
Heterogeneous	0.88	0.84
Solid Angle	0.90	0.86
21:31 UTC		
Homogeneous	0.86	0.82
Heterogeneous	0.89	0.85
Solid Angle	0.93	0.90
CAR (Local)	**0.82 ± 0.036**	**0.77 ± 0.036**
SSFR (at Cloud Top)	0.90 ± 0.038	0.82 ± 0.038
Simulation		
(Local),		
No Aerosol	0.85	0.82
With Aerosol	**0.84**	**0.82**
(At Cloud Top),		
No Aerosol	0.88	0.82
With Aerosol	0.87	0.82

Table 1 – Comparison of albedos. The "local" albedo is the ratio of the upwelling irradiance at cloud top to the estimated downwelling irradiance at the top of the atmosphere. The assigned uncertainty corresponds to one standard deviation in the observation, and does not include any uncertainty which is inherent in retrieval process. The change in the AirMISR retrieval due to "within scene" variability is less than the calibration uncertainty of 3%. It must be stressed that all of the measurements correspond to somewhat different times and different regions of the cloud field. With that said, one would expect the AirMISR 21:02 UTC and the CAR measurements to be in the closest agreement.

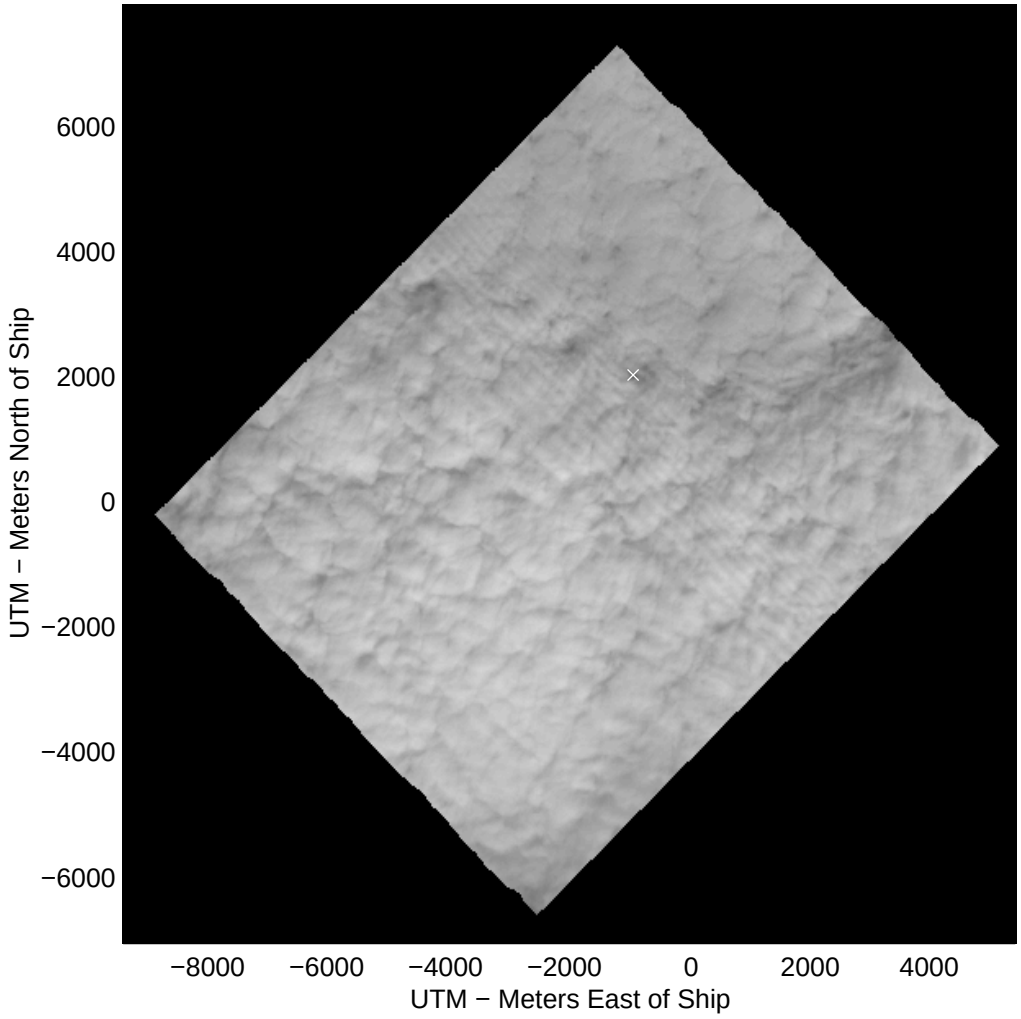
6000
4000
2000
0
−2000
−4000
−6000
UTM − Meters North of Ship
−8000
−6000
−4000
−2000
0
2000
4000
UTM − Meters East of Ship

Figure 1a

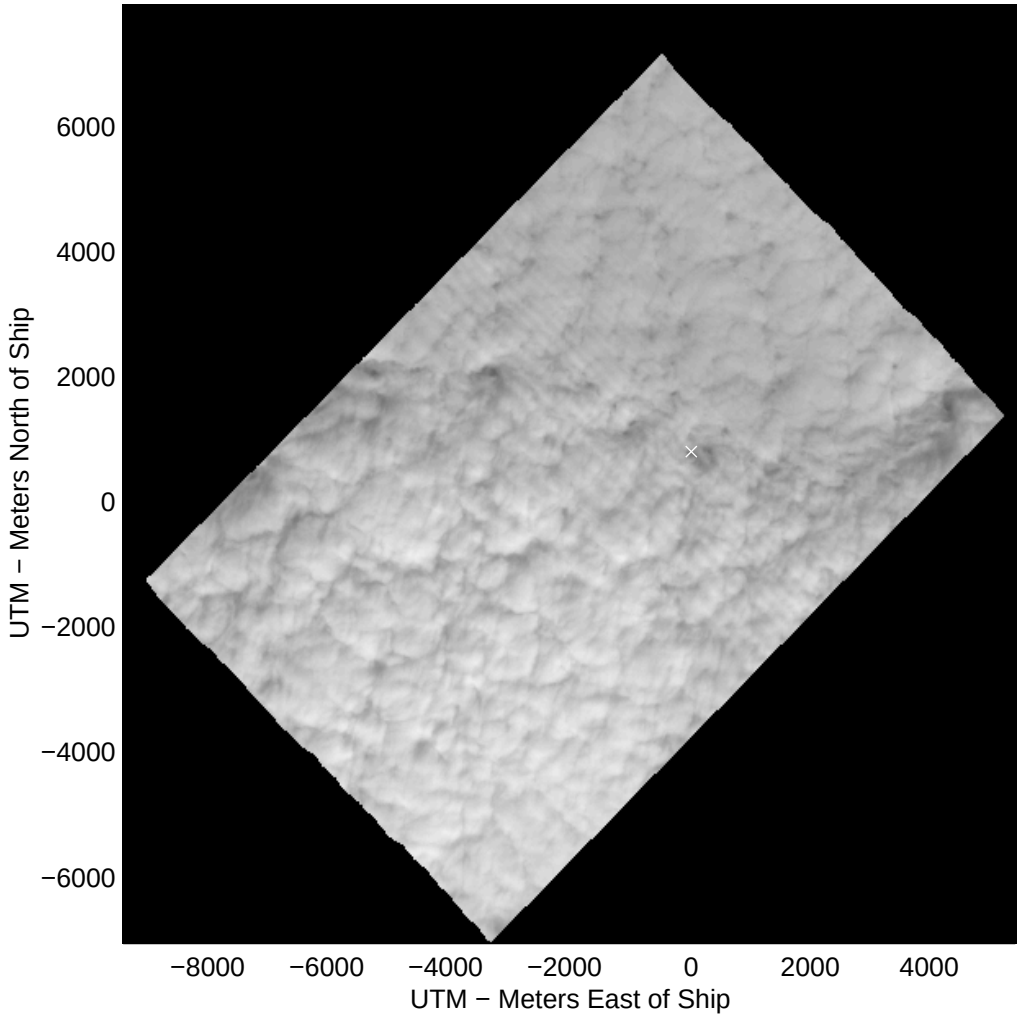
6000
4000
2000
0
−2000
−4000
−6000
UTM − Meters North of Ship
−8000
−6000
−4000
−2000
0
2000
4000
UTM − Meters East of Ship

Figure 1b

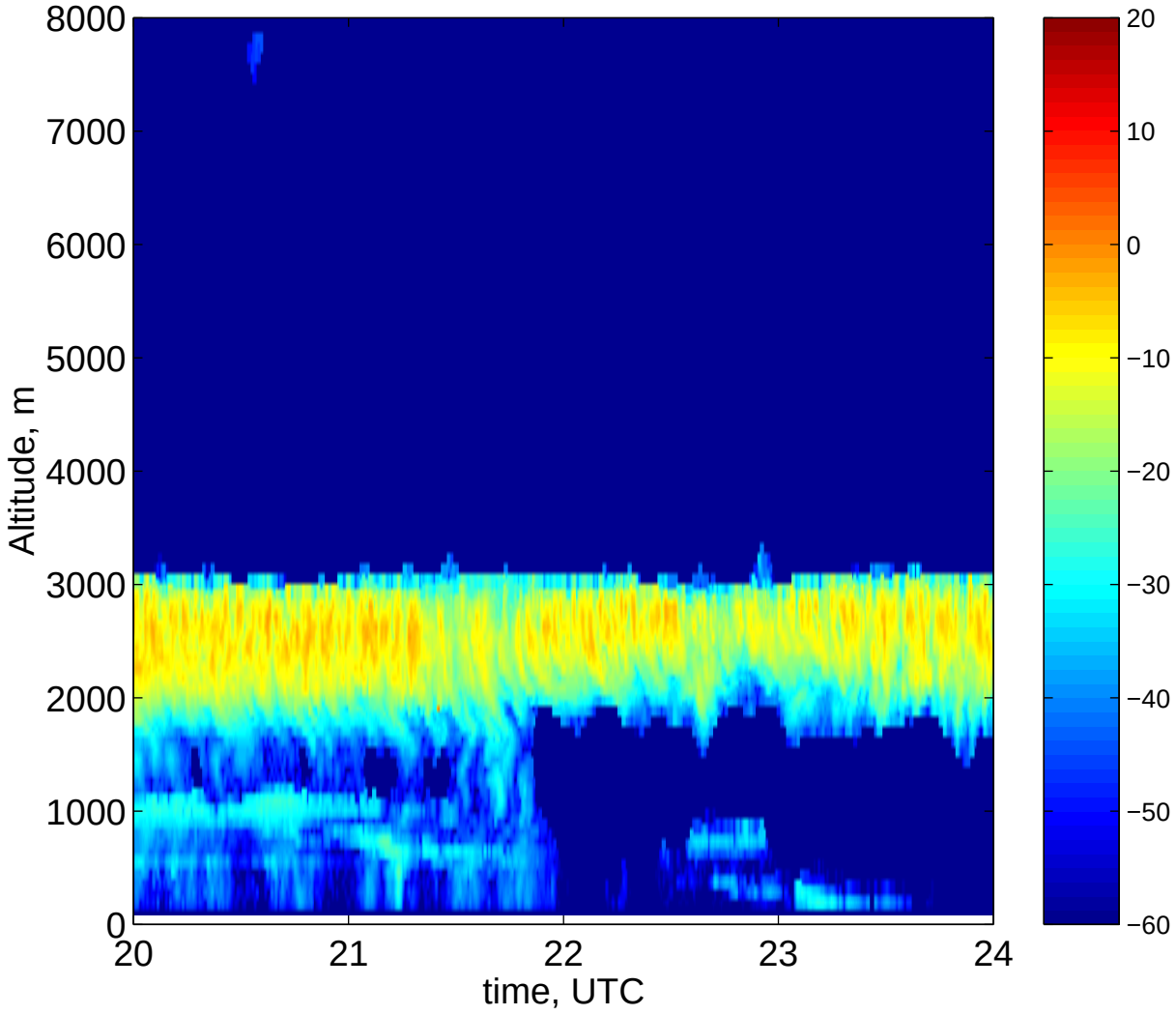
8000
7000
6000
5000
4000
3000
2000
1000
0
Altitude, m
20
21
22
23
24
time, UTC
20
10
0
−10
−20
−30
−40
−50
−60

Figure 2

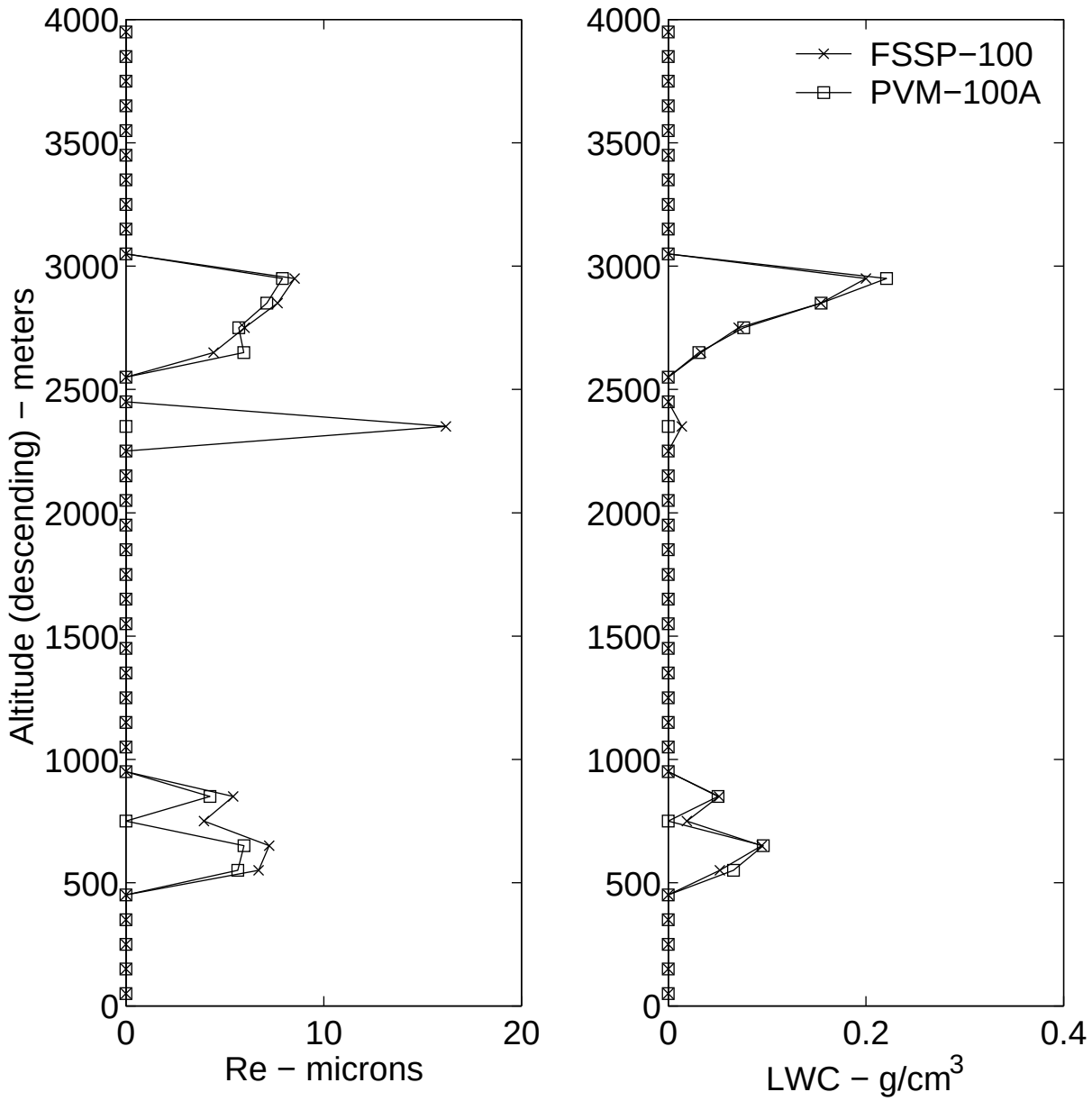
4000
3500
3000
2500
2000
1500
1000
500
0
Altitude (descending) – meters
0
10
20
Re − microns
FSSP−100
PVM−100A
0
0.2
0.4
LWC − g/cm3

Figure 3

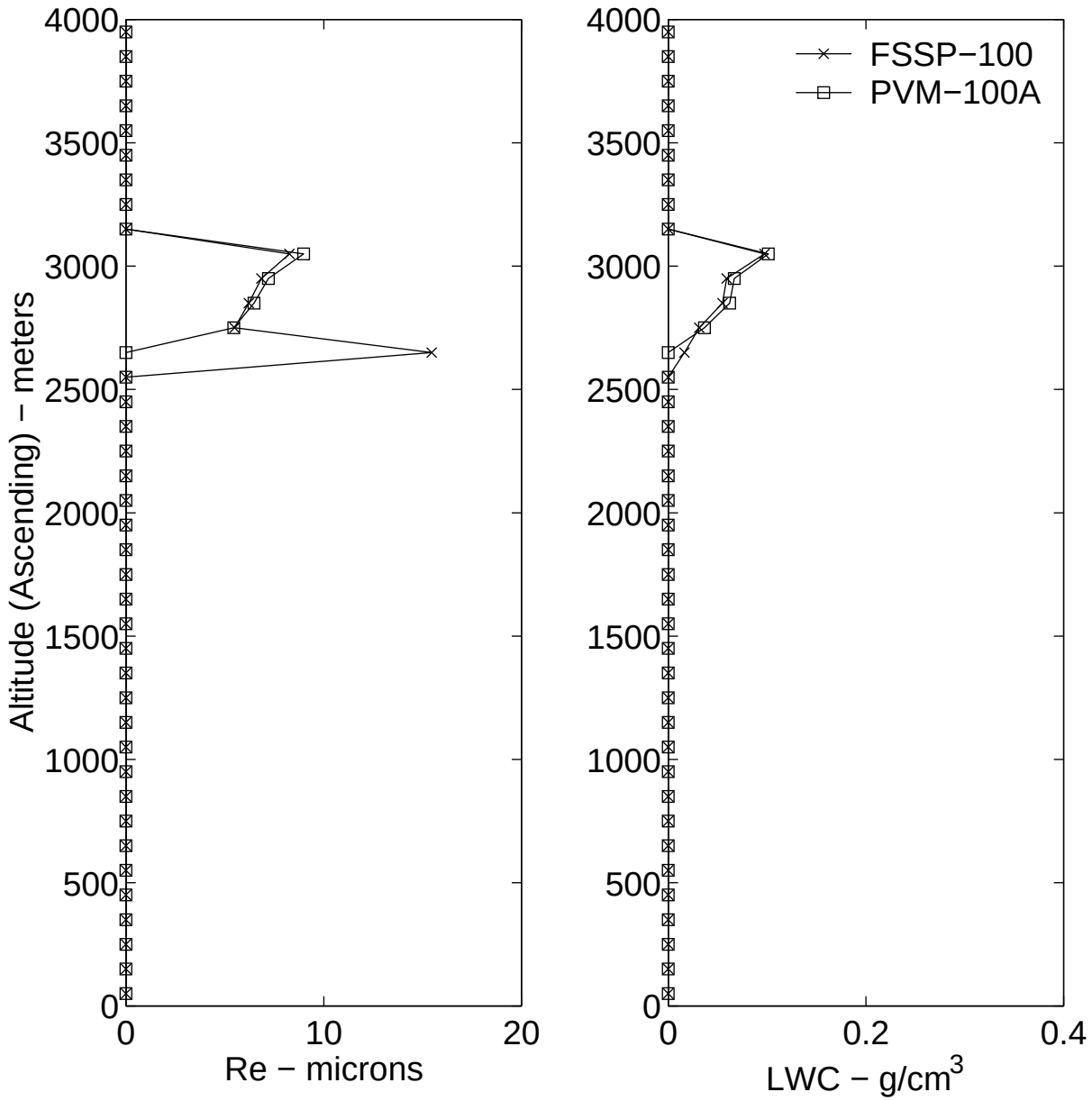
4000
3500
3000
2500
2000
1500
1000
500
0
Altitude (Ascending) − meters
0
10
20
Re − microns
FSSP−100
PVM−100A
0
0.2
0.4
LWC − g/cm3

Figure 4

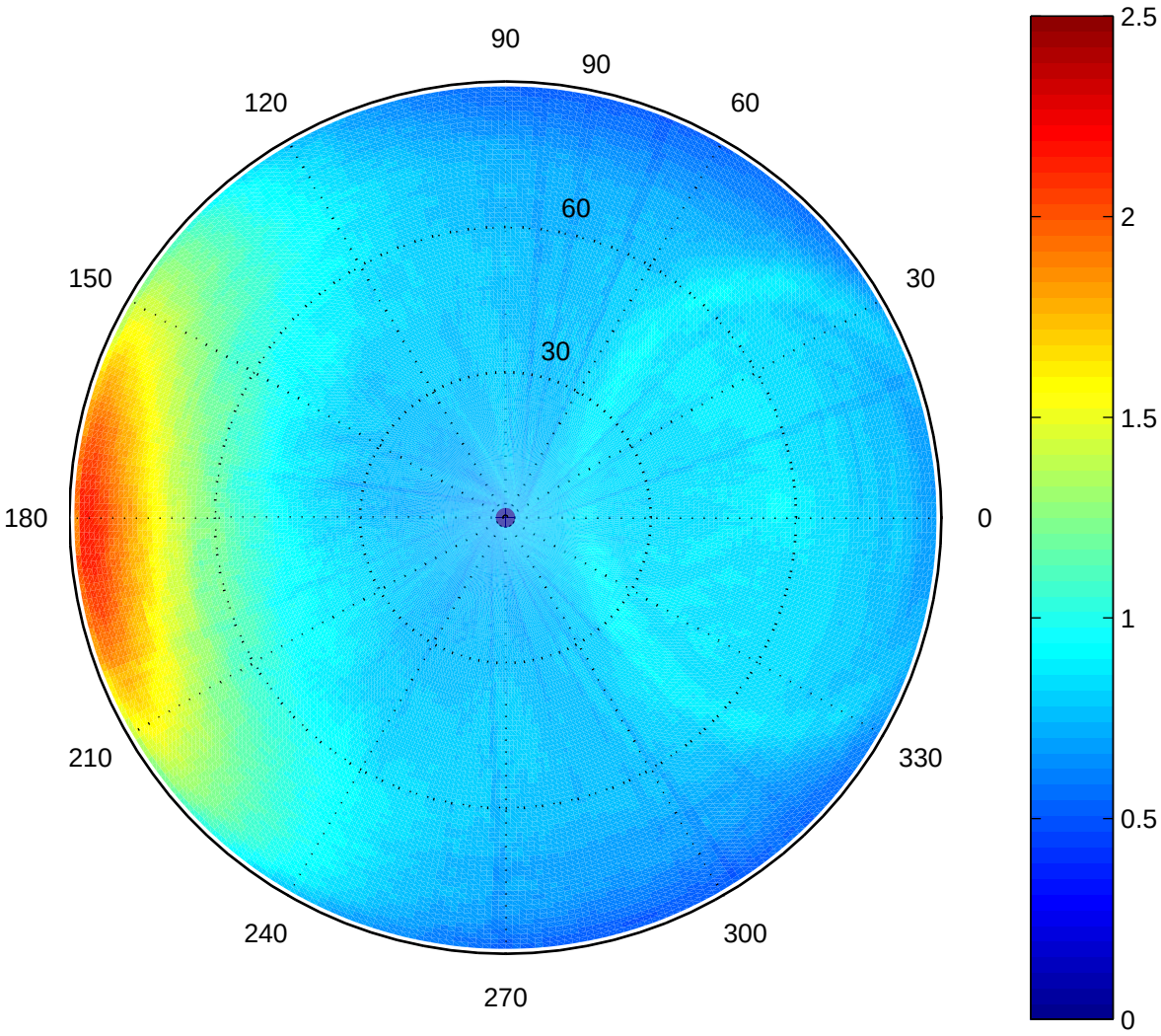

Figure 5

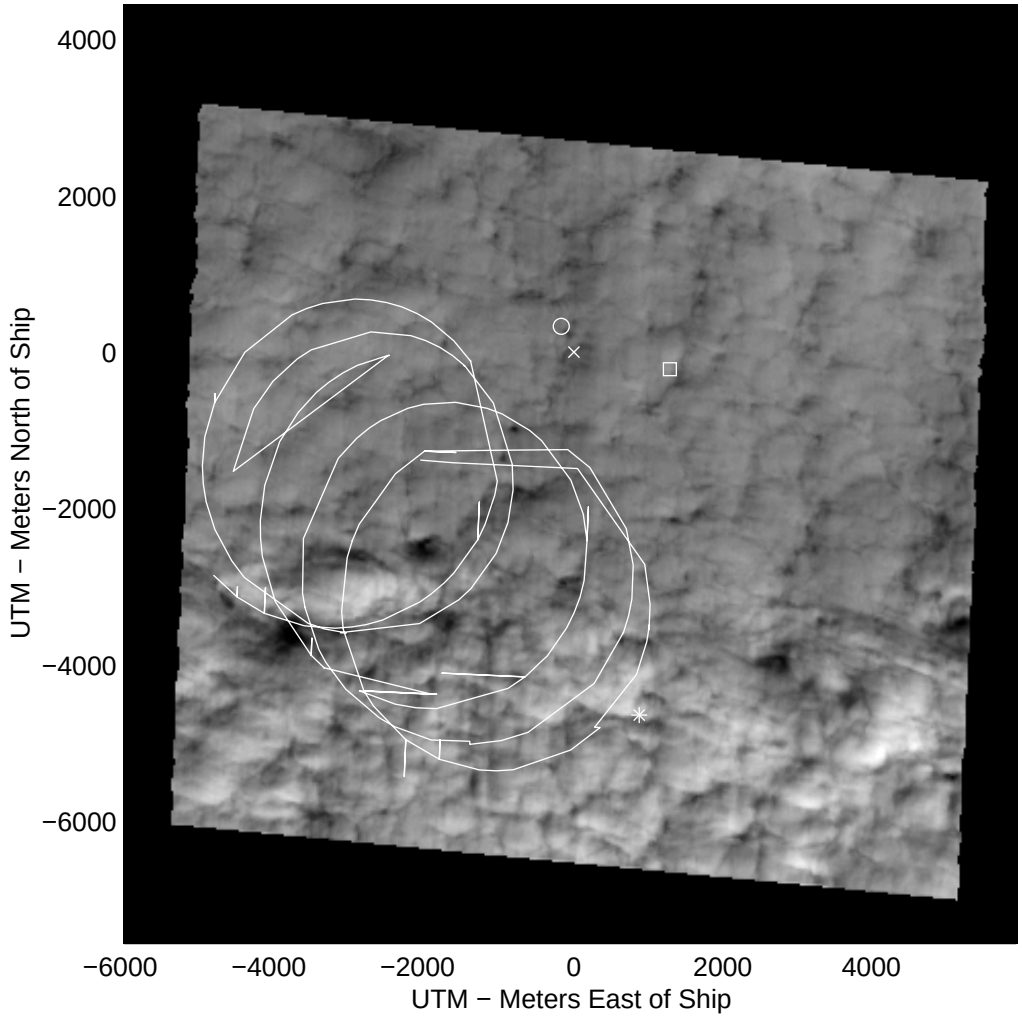
4000
2000
0
−2000
−4000
−6000
UTM − Meters North of Ship
−6000
−4000
−2000
0
2000
4000
UTM − Meters East of Ship

Figure 6

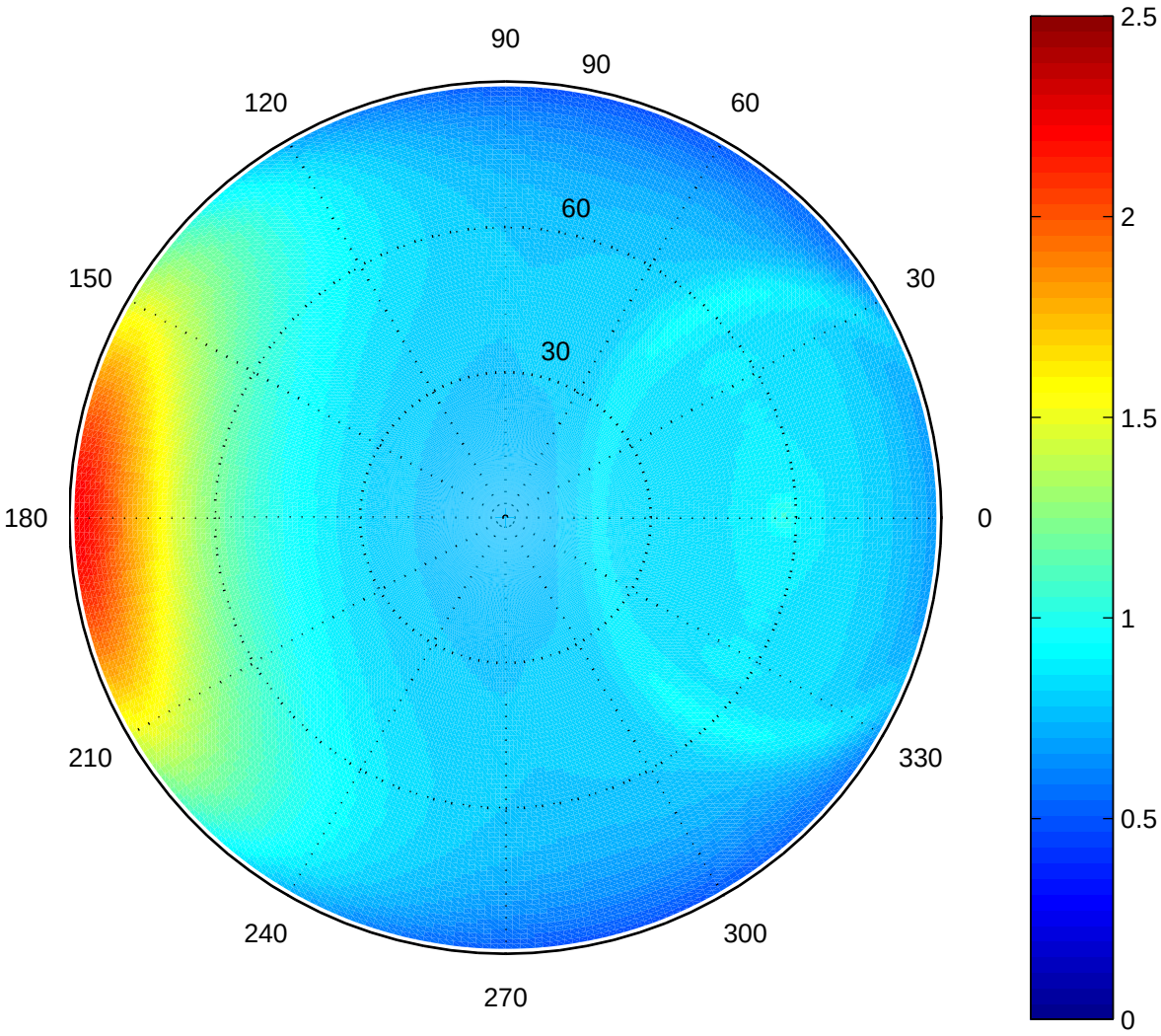

Figure 7

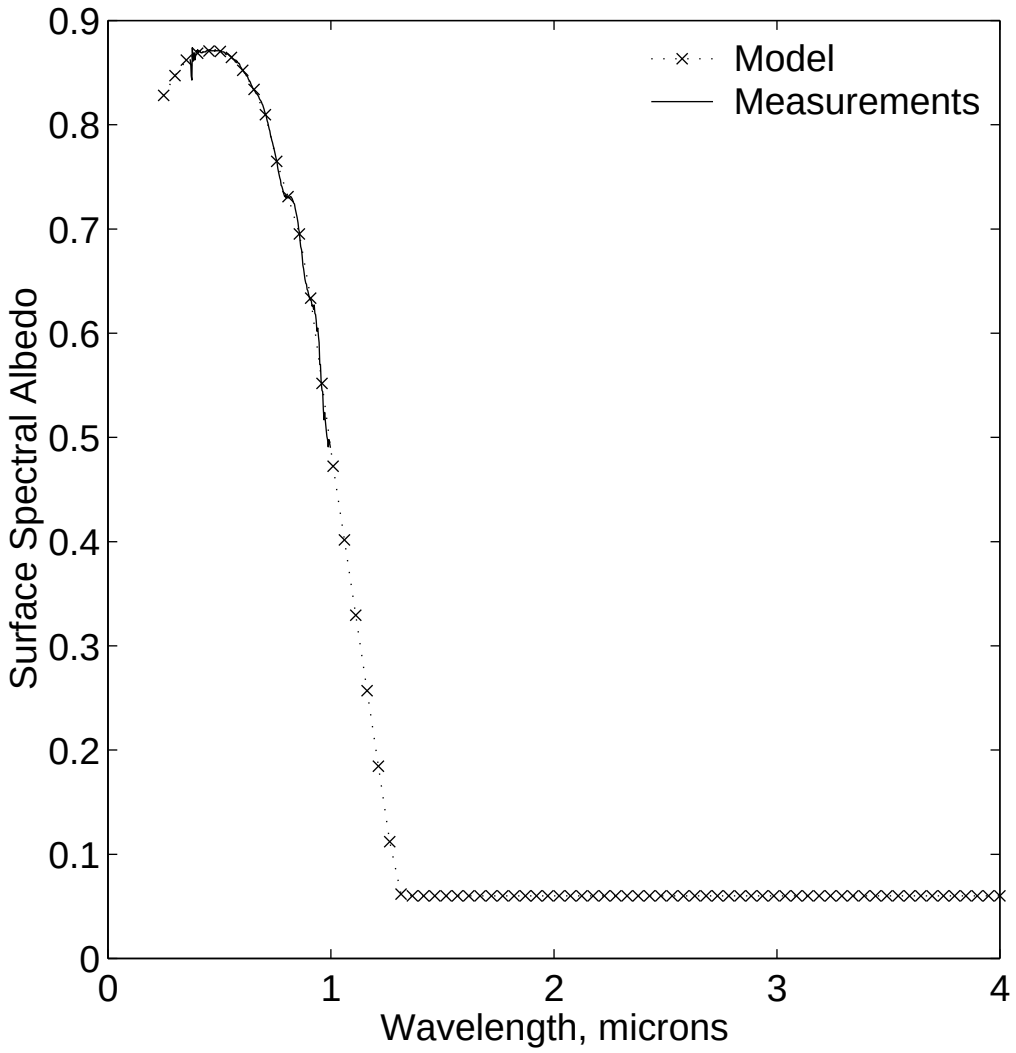
Model
Measurements
Surface Spectral Albedo
Wavelength, microns
0
0.1
0.2
0.3
0.4
0.5
0.6
0.7
0.8
0.9
0
1
2
3
4

Figure 8

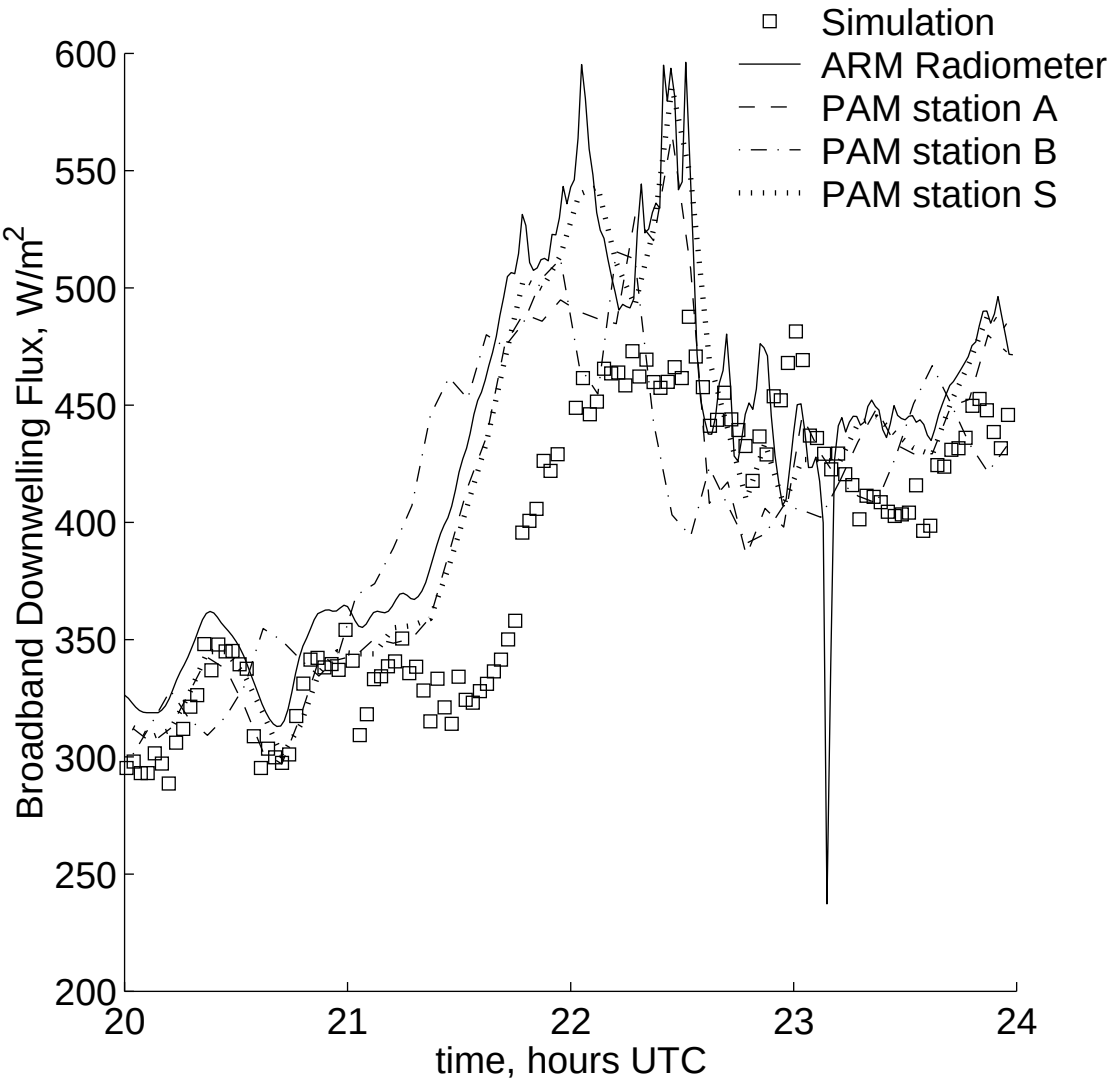
Simulation
ARM Radiometer
PAM station A
PAM station B
PAM station S
Broadband Downwelling Flux, W/m2
time, hours UTC
600
550
500
450
400
350
300
250
200
20
21
22
23
24

Figure 9

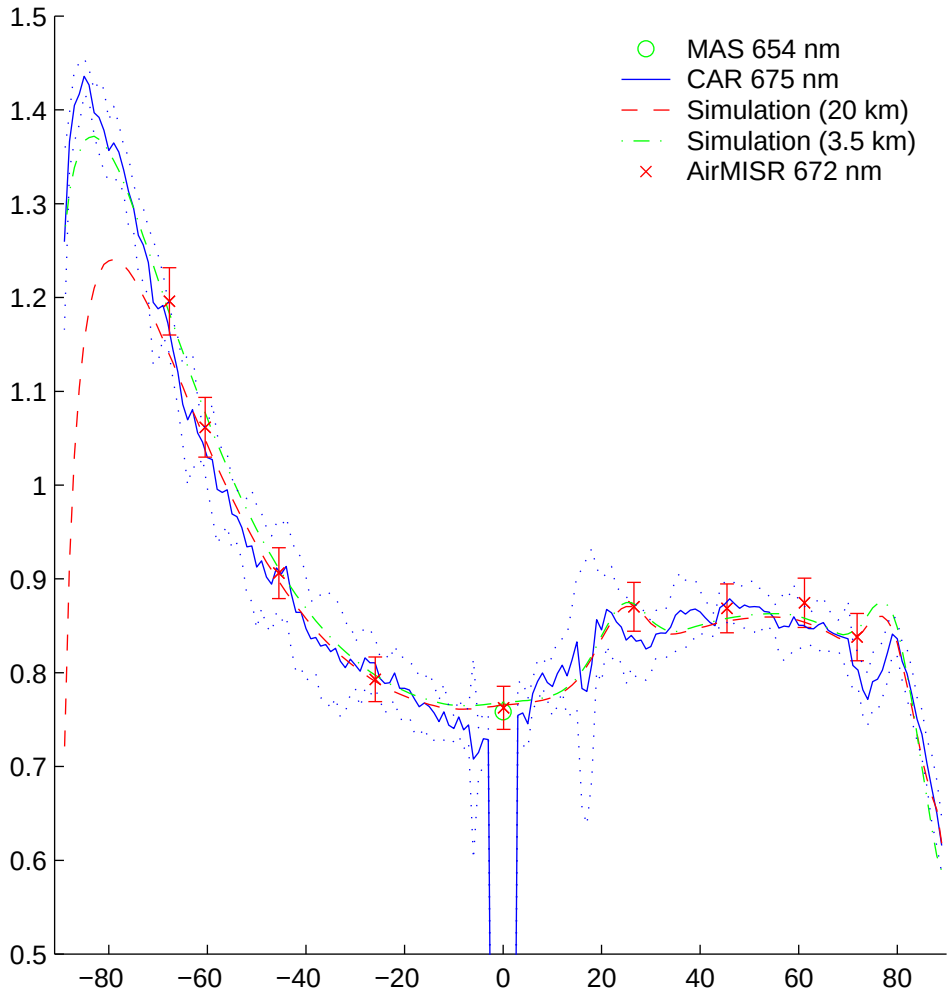
MAS 654 nm
CAR 675 nm
Simulation (20 km)
Simulation (3.5 km)
AirMISR 672 nm
1.5
1.4
1.3
1.2
1.1
1
0.9
0.8
0.7
0.6
0.5
−80
−60
−40
−20
0
20
40
60
80

Figure 10

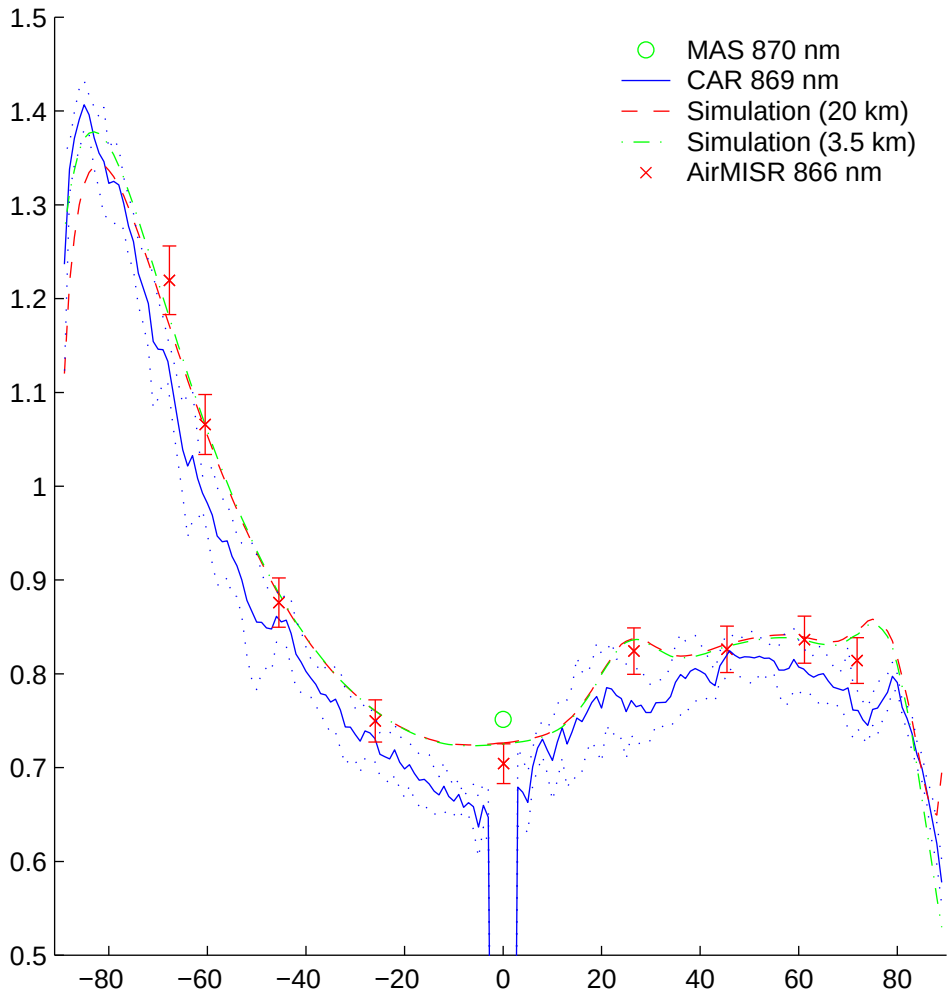
MAS 870 nm
CAR 869 nm
Simulation (20 km)
Simulation (3.5 km)
AirMISR 866 nm
1.5
1.4
1.3
1.2
1.1
1
0.9
0.8
0.7
0.6
0.5
−80
−60
−40
−20
0
20
40
60
80

Figure 11

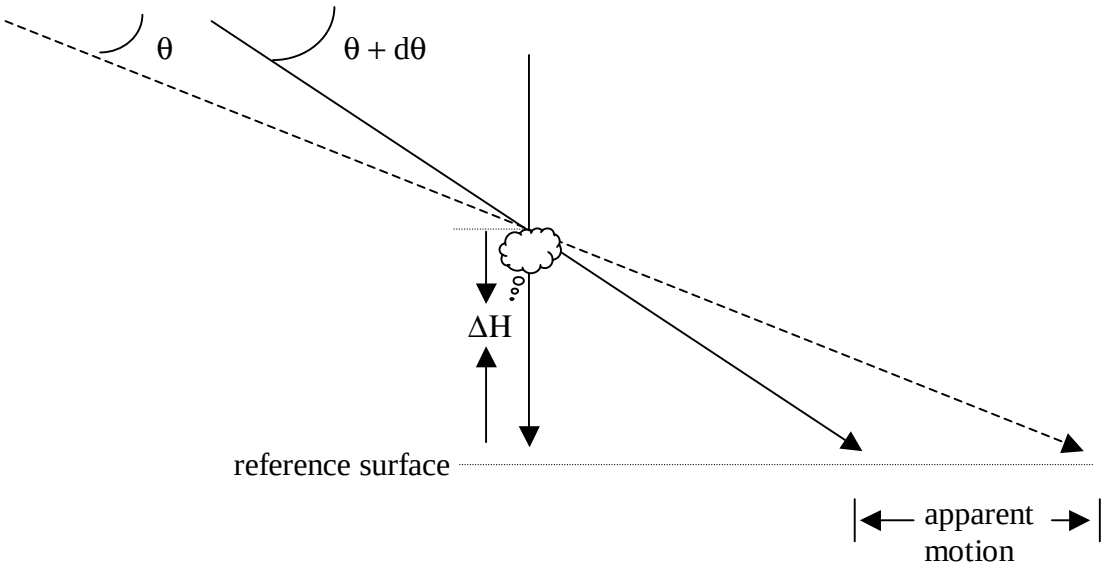

Figure 12

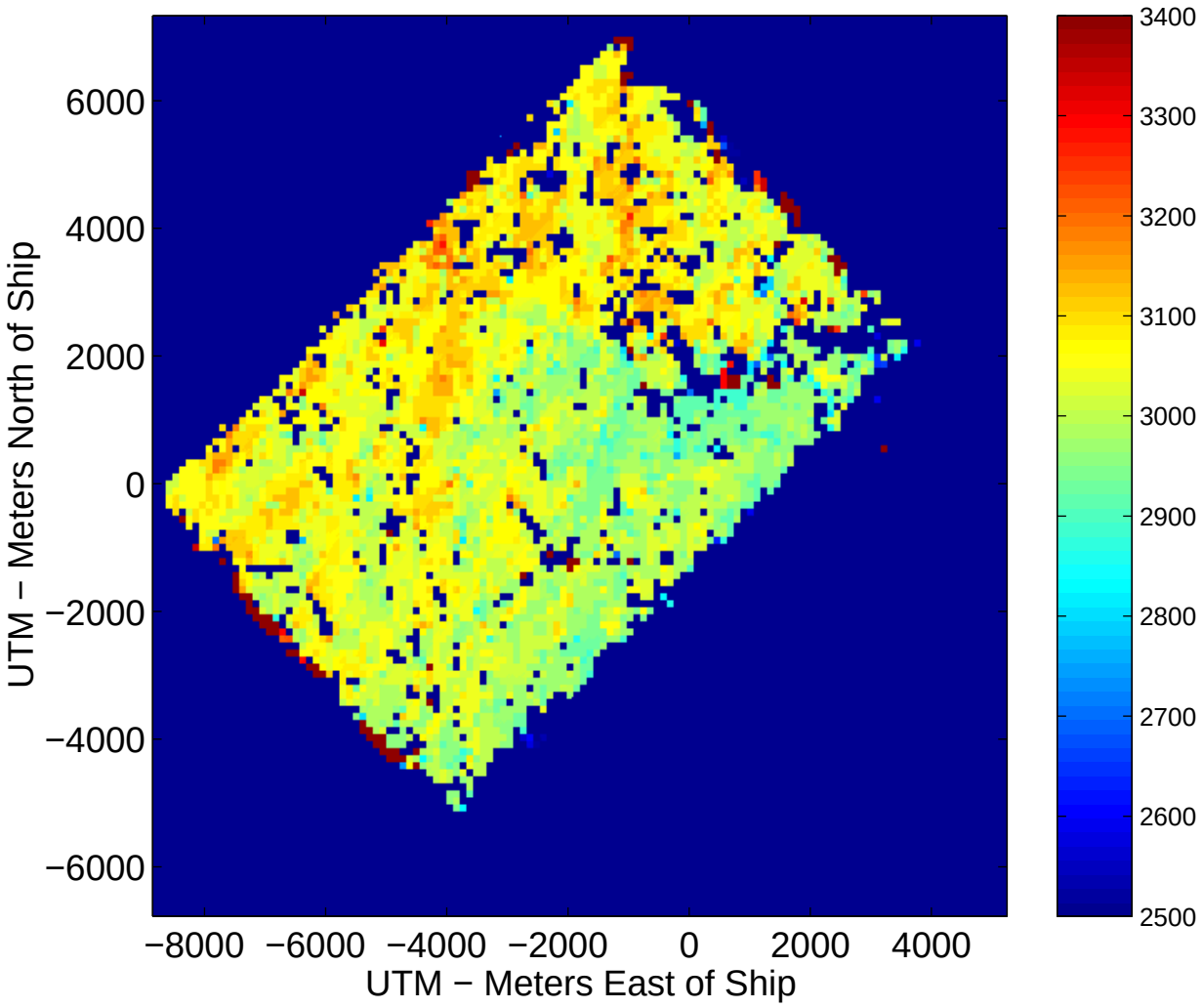
6000
4000
2000
0
−2000
−4000
−6000
UTM − Meters North of Ship
−8000
−6000
−4000
−2000
0
2000
4000
UTM − Meters East of Ship
3400
3300
3200
3100
3000
2900
2800
2700
2600
2500

Figure 13

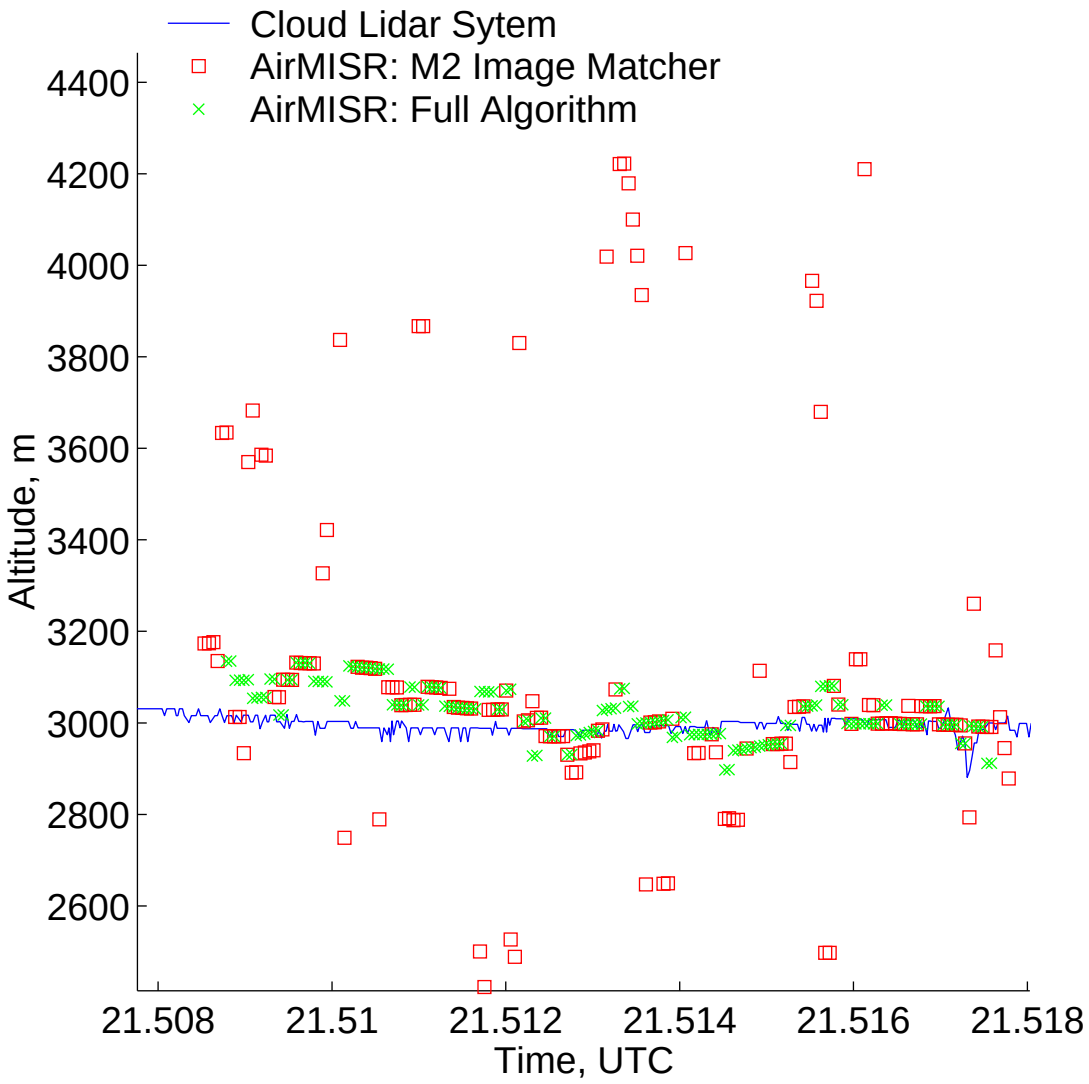
Cloud Lidar Sytem
AirMISR: M2 Image Matcher
AirMISR: Full Algorithm
Altitude, m
4400
4200
4000
3800
3600
3400
3200
3000
2800
2600
21.508
21.51
21.512
21.514
21.516
21.518
Time, UTC

Figure 14

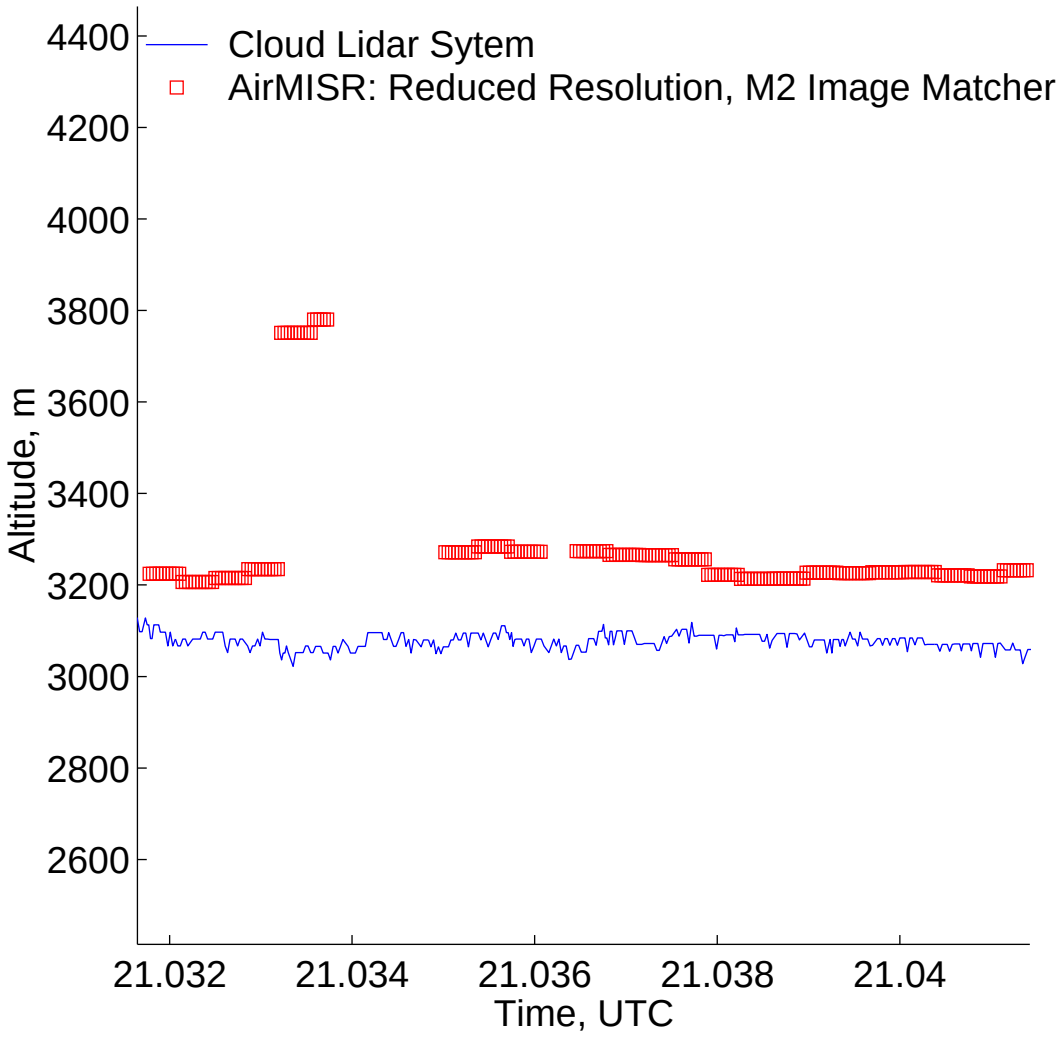
Cloud Lidar Sytem
AirMISR: Reduced Resolution, M2 Image Matcher
Altitude, m
4400
4200
4000
3800
3600
3400
3200
3000
2800
2600
21.032
21.034
21.036
21.038
21.04
Time, UTC

Figure 15